Supporting Information

A ship-in-a-bottle architecture transmission metal hydroxides@conducting MOF on carbon nanotube yarn for ultra-stable quasi-solid-state supercapacitors

Qingli Xu[1], Xia Liu[2], Juan Zhang[1], Yifei Xu[3], Mi Zhou[4], Jiaxin Li[3], Minzhi Du[1], Kun Zhang[3], Xiangyu Qian[1], Bo Xu[4], Xinhou Wang[1], Bingjie Wang[3*], Kun Zhang[1*]

[1]*Key Laboratory of Textile Science & Technology of Ministry of Education, College of Textiles, Donghua University, 2999 North Renmin Road, Shanghai 201620, P.R. China;* E-mail: kun.zhang@dhu.edu.cn

[2]*State Key Laboratory of Chemo/Biosensing and Chemometrics, Hunan University, Changsha 410082, China.*

[3]*Laboratory of Advanced Materials, State Key Laboratory of Molecular Engineering of Polymers, Department of Macromolecular Science, Fudan University, 2205 Songhu Road, Shanghai 200438, P.R. China;* E-mail: wangbingjie@fudan.edu.cn

[4]*College of Chemistry, Chemical Engineering and Biotechnology, Donghua University, 2999 North Renmin Road, Shanghai 201620, P.R. China.*

Contents

Supplementary Figure 13 | CV and GCD curves of (**a**, **b**) $Ni(OH)_2$@CNTY SC, (**c**, **d**) $Ni_3(HITP)_2$@CNTY SC, (**e**, **f**) $Ni(OH)_2$@$Ni_3(HITP)_2$@CNTY SC and (**g**, **h**) $Co(OH)_2$@$Ni_3(HITP)_2$@CNTY SC.

Supplementary Figure 14 | *b*-value and bar chart indicating the percentages of capacitive contribution of (**a**, **b**) $Ni(OH)_2$@CNTY SC, (**c**, **d**) $Ni_3(HITP)_2$@CNTY SC, (**e**, **f**) $Ni(OH)_2$@$Ni_3(HITP)_2$@CNTY SC and (**g**, **h**) $Co(OH)_2$@$Ni_3(HITP)_2$@CNTY SC from 5 to 200 mV/s.

Supplementary Figure 15 | (**a**) The calculated capacitance of CNTY-based electrodes. (**b**) Energy density and power density of CNTY-based electrodes.

Supplementary Figure 16 | (**a**) Nyquist-plot of TMH NPs@$Ni_3(HITP)_2$@CNTY SCs with raw data as a solid line and fitting as short dot line. (b) Electrical equivalent circuit used for fitting the experimental EIS data. Note: The Warburg diffusion element W_o is a function of three parameters: *W*-*R*, the Warburg diffusion impedance; *W*-*T*, the diffusion time constant, and *W*-*P*, the phase factor ($0 < W\text{-}P < 1$).

Supplementary Figure 17 | GCD curves of (**a**, **b**) $Ni(OH)_2$@$Ni_3(HITP)_2$@CNTY SC and (**c**, **d**) $Co(OH)_2$@$Ni_3(HITP)_2$@CNTY SC with different bending angles and after bending 3000 cycles at 90°. Notes: The insets of (b) and (d) are FESEM images of $Ni(OH)_2$@$Ni_3(HITP)_2$@CNTY SC and $Co(OH)_2$@$Ni_3(HITP)_2$@CNTY SC after bending 3000 cycles at 90°, respectively.

Supplementary Figure 18 | XRD patterns of CNT film-based samples after 10000 cycles in two-electrode system. Note: The CNT which forms CNTY and CNT film is not different.

Supplementary Figure 19 | The mechanical property of CNTY-based samples.

Supplementary Figure 20 | Galvanostatic charging/discharging curves of the assembled SCs connected in series.

Supplementary Figure 21 | The power requirement of smart devices and the integrated YSC

Supplementary Table 1 | The conductivity of CNTY-based electrodes

Supplementary Table 2 | Comparison of $Ni(OH)_2$-based symmetric supercapacitors

Supplementary Table 3 | Resistance values obtained by fitting the equivalent circuit to the EIS plots for TMH NPs@$Ni_3(HITP)_2$@CNTY SCs

Supplementary References

Supplementary Note 1

Materials and Experiments

1.1 Materials.

2,3,6,7,10,11-hexabromo-triphenylene was purchased from Zhengzhou Alpha Chemical Co., Ltd., China. Benzophenone imine was purchased from Brilliant Technology Co., Ltd., China. Silica gel was purchased from Aladdin Reagent (Shanghai) Co., Ltd., China. Tris (dibenzylideneacetone) dipalladium (0), sodium *tert*-butoxide, *rac*-BINAP and hexane were purchased from TCI (Shanghai) Chemical Industry Development Co., Ltd., China. Hydrochloric acid (HCl), celite, dichloromethane (CH_2Cl_2), ethyl acetate (AcOEt) and tetrahydrofuran (THF) were purchased from Shanghai Titan Technology Co., Ltd., China. Toluene, ethanol, sulfuric acid (H_2SO_4, 98 wt%), nickel (II) chloride hexahydrate puratrem ($NiCl_2 \cdot 6H_2O$), nickel (II) sulfate hexahydrate puratrem ($NiSO_4 \cdot 6H_2O$), ammonia and potassium hydroxide (KOH) were purchased from Sinopharm Chemical Reagent Co., Ltd., China. Polyvinyl alcohol 1788 (PVA) was purchased from Sinopharm Chemical (oruchem) Reagent Co., Ltd., China. Cobalt chloride ($CoCl_2$, 99.7%) was purchased from Alfa Aesar. Carbon nanotube yarn (CNTY) was provided by Fudan University. CNT film was purchased from Chengdu Organic Chemistry Co., LTD, Chinese Academy of Sciences. Deionized (DI) water was made with Master-Q15 (resistivity ~18.3 MΩ·cm). All materials were used as received without further purification.

1.2 Preparation of 2,3,6,7,10,11-hexaaminotriphenylene hexahydrochloride (HATP·6HCl).

HATP·6HCl was prepared according to the reported reference.[1] In detail, a toluene solution (50 mL) of tris (dibenzylideneacetone) dipalladium(0) (0.448 g, 0.49 mmol) and *rac*-BINAP (0.607 g, 0.98 mmol) was degassed by four freeze-pump-thaw cycles, purged with Ar gas and stirred at 110 ℃ for 30 min. After cooling at room temperature, the mixture was added with benzophenone imine (2.65 mL, 15.77 mmol), 2,3,6,7,10,11-hexabromo-triphenylene (1.419 g, 2.02 mmol) and sodium *tert*-butoxide (1.516 g, 15.77 mmol), stirring at 110 ℃ overnight. Then, the mixture was cooled at room temperature, following diluted, filtered through a pad of celite, and evaporated to dry. The residue was subjected with CH_2Cl_2 to column

chromatography on silica gel with AcOEt/hexane (1:4) as eluent. The last fraction was collected and evaporated to dry to obtain the yellow powder (2.001 g, 1.53 mmol). Finally, a 2.0 M aqueous HCl solution (0.5 mL, 1.0 mmol) was added to a THF solution (10 mL) of the obtained powder (0.219 g, 0.17 mmol). The mixture was stirred at room temperature for 30 min. The precipitate was isolated by centrifugation, washed with hexane (5.0 mL x 3) and dried under vacuum, to finally obtain light yellow HATP·6HCl.

1.3 Preparation of CNTY coated with $Ni_3(HITP)_2$ ($Ni_3(HITP)_2$@CNTY).

Before functionalizing pristine CNTY with diameter of 120 ~um, CNTY was immersed in HCl for 3 h and then washed with DI water to remove impurity. Subsequently, $Ni_3(HITP)_2$@CNTY was prepared by the following steps. 6.69 mg (0.001 mol/L) of HATP·6HCl ligand was dispersed in 15 ml DI water, and stirred for 2 h. Then the as-prepared CNTY was immersed in the above solution under low stirring speed for one day, two days and four days, respectively. A solution of 4.44 mg of $NiCl_2·6H_2O$ in 2 ml DI water was added to the above solution. Then 60 μl of concentrated aqueous ammonia ($NH_3·H_2O$) was added to the mixture. The mixture was stirred in a flask under air bubbling for 1 h at 60 °C, continued to be stirred for an additional 2 h at 60 °C. Finally, the prepared $Ni_3(HITP)_2$@CNTY samples labeled as $Ni_3(HITP)_2$@CNTY, $Ni_3(HITP)_2$@$CNTY_{(2)}$ and $Ni_3(HITP)_2$@$CNTY_{(4)}$ were washed with DI water and ethanol for 3 times, respectively, and dried in vacuum oven for 12 hours.

1.4 Preparation of $Ni_3(HITP)_2$@CNTY loaded with $Ni(OH)_2$ NPs ($Ni(OH)_2$@$Ni_3(HITP)_2$@CNTY).

The $Ni_3(HITP)_2$@CNTY was immersed in 0.5 mol/L $NiSO_4·6H_2O$ for 4 h at 45 °C, and washed with DI water for 1 time to remove nickel ions on the surface of $Ni_3(HITP)_2$@CNTY. Then, $Ni(OH)_2$@$Ni_3(HITP)_2$@CNTY was composited by being placed in 0.3 M ammonia gas surrounding at 25 °C for 15 min. The obtained $Ni(OH)_2$@$Ni_3(HITP)_2$@CNTY was washed 3 times with DI water, and then dried at 50 °C under vacuum for 12 h.

1.5 Preparation of $Ni_3(HITP)_2$@CNTY loaded with $Co(OH)_2$ NPs ($Co(OH)_2$@$Ni_3(HITP)_2$@CNTY).

The $Ni_3(HITP)_2$@CNTY was immersed in 0.3 mol/L $CoCl_2$ for 4 h at 45 °C, and washed with DI water for 1 time to remove cobalt ions on the surface of $Ni_3(HITP)_2$@CNTY. Then

$Co(OH)_2$@$Ni_3(HITP)_2$@CNTY was composited by being placed in 0.05 M ammonia gas surrounding at 25 °C for 15 min. The obtained $Co(OH)_2$@$Ni_3(HITP)_2$@CNTY was washed 3 times with DI water, and then dried at 50 °C under vacuum for 12 h.

1.6 Preparation of CNTY coated with $Ni(OH)_2$ ($Ni(OH)_2$@CNTY).

The CNTY was immersed in 0.5 mol/L $NiSO_4 \cdot 6H_2O$ for 4 h at 45 °C. Then the prepared CNTY was placed in 0.3 M ammonia gas surrounding at 25 °C for 15 min. The obtained $Ni(OH)_2$@CNTY was washed 3 times with DI water and dried at 50 °C under vacuum for 12 h.

1.7 Preparation of $Ni_3(HITP)_2$ and $Co(OH)_2$@$Ni_3(HITP)_2$ for cryogenic transmission electron microscopy (cryo-TEM).

First, a solution of $NiCl_2 \cdot 6H_2O$ (13.32 mg) in 2 ml DI water was added to a solution of HATP·6HCl (20.07 mg) in 45 ml DI water. Second, 191.25 ul of $NH_3 \cdot H_2O$ was added to the mixture. Third, the mixture was stirred in a flask under air bubbling for 1 h at 60 °C, continued to be stirred for an additional 2 h at 60 °C. Finally, the above mixture was washed 6 times with DI water, the final $Ni_3(HITP)_2$ was dissolved in 13 ml DI water. It should be noted that 20.07 mg of HATP·6HCl theoretically yields 15.05 mg of $Ni_3(HITP)_2$. Besides, we assume that the mass loss of $Ni_3(HITP)_2$ is 2 mg during washing process. Therefore, the concentration of $Ni_3(HITP)_2$ solution is ~1 mg/ml, which can be used for cryo-TEM characterization. For the preparation of $Co(OH)_2$@$Ni_3(HITP)_2$, a solution of $CoCl_2$ in 2 ml of DI water was added to 10 ml of the above $Ni_3(HITP)_2$ solution at first. Then, the mixture was stirred for 4 h at 45 °C, and 1.34 ml diluted $NH_3 \cdot H_2O$ (0.05 M) was added to the mixture and continued to be stirred for 12 h at 25 °C. The above mixture was washed 6 times with DI water, the final $Ni_3(HITP)_2$ was dissolved in 10 ml DI water at last.

1.8 Assembly process of flexible yarn-based supercapacitors (YSCs).

The fabrication steps of YSCs in aqueous electrolyte were as follows. 10 g PVA was dissolved in 100 ml DI water at 90 °C. The PVA solution was stirred for 30 min until complete dissolution. 0.98 g H_2SO_4 was gradually added into PVA solution to form H_2SO_4/PVA gel electrolyte. To assemble all-solid-state YSC, two yarn electrodes were immersed in 1 M H_2SO_4 /PVA gel electrolyte and later laid parallel on a polyethylene terephthalate (PET) substrate. The

ends of each yarn were glued onto a polished copper foil by silver paste with yarn interval at ~2 mm. Pristine CNTY and $Ni_3(HITP)_2$@CNTY with different immersing time were assembled into YSCs and then solidified for 12 h at room temperature. Alkaline electrolyte of 2 M KOH/PVA was prepared to protect the ternary electrodes. 1 g PVA was dissolved in 8 ml DI water at 90 °C to obtain PVA solution. 1.12 g KOH was dissolved in 2 ml DI water to obtain KOH solution. Then the KOH solution was dropped into the PVA solution at room temperature with vigorous stirring to make KOH/PVA gel electrolyte. $Ni(OH)_2$@CNTY, $Ni_3(HITP)_2$@CNTY, $Ni(OH)_2$@$Ni_3(HITP)_2$@CNTY and $Co(OH)_2$@$Ni_3(HITP)_2$@CNTY electrodes were assembled and tested in KOH/PVA gel electrolyte.

Supplementary Note 2

Measurements and Characterizations

The surface morphology of all samples was characterized at low/high resolution with a field emission scanning electron microscope (FESEM, Hitachi, SU8010 series, 5 kV (morphology), 10 kV (EDS)) without sputter coating. The morphology of all prepared single CNT samples was measured with a transmission electron microscope (TEM, J2100F). High-resolution TEM images (HRTEM) were obtained with a JEOL JEM2100F microscope. In addition, all samples were cut into small pieces, respectively. Then the above pieces were put in ethanol and ultrasonicated until all pieces were divided into bundles or single CNT to obtain TEM samples.

The morphology of $Ni_3(HITP)_2$ and $Co(OH)_2$@$Ni_3(HITP)_2$ was also characterized by cryogenic transmission electron microscopy (cryo-TEM). The cryo-TEM samples were prepared by applying 3 μL of solution samples on Quantifoil cryo-TEM grids. The grids were blotted for 3 secs and vitrified using a FEI Mark IV Vitrobot, and then transferred to a Fishione Model 2250 cryoholder for cryo-TEM imaging. The imaging was performed using a Tecnai G20 TEM equipped with LaB6 electron gun and a 2k x 2k Gatan CCD camera, with a defocus value of 3 μm and a dose rate of 20 $e^-/Å^2$ per frame.

X-ray diffraction (XRD) patterns of all samples were obtained from X-ray diffractometer using Cu Kα radiation (λ = 1.54056 Å) (RIGAKU D/Max-2550PC, 40 kV, 200 mA). All samples were scanned at a step size of 2°/min from $2\theta = 3°$ to $2\theta = 90°$. Raman spectra of all

samples were recorded by using Bruker Multi RAM, Germany over 500-3500 cm^{-1} excited with Argon 488 nm laser source obtained at room temperature. Fourier transform infrared spectroscopy (FTIR), with a resolution of 2 cm^{-1} and an average of 25 scans, was conducted on a Nicolet NEXUS-670 to characterize the chemical structure of all samples. X-ray photoelectron spectroscopy (XPS) spectra of prepared samples were collected on an ESCALAB250Xi. Nitrogen (N_2) adsorption-desorption isotherms were measured at -77.3 K with a Micromeritics ASAP 2460 static volumetric gas adsorption instrument. Prior to testing, the samples were degassed at 80 °C for 12 h. The specific surface area was calculated based on the Brunauer–Emmett–Teller (BET) technique. The pore size distributions were obtained by means of density functional theory (DFT). Image J software was used to measure the diameter (*D*) along the longitudinal direction of yarn from FESEM images at 10 different locations. The mechanical property was tested by an electronic single fiber strength tester (LLY-06 EDC).

Supplementary Note 3

Computational Method and Modeling

All calculations were performed within the framework of density functional theory (DFT) as implemented in the Vienna Ab initio Simulation Package (VASP).[2-3] The exchange-correlation interactions were treated by generalized gradient approximation (GGA) parameterized by Perdew, Burke and Ernzerhof (PBE).[4] We described the interaction between ions and electrons using the projected augmented wave (PAW) with an energy cutoff of 500 eV.[5-6] The atomic positions were optimized by the conjugate gradient algorithm until the force on each atom was less than 0.01 eV/Å. In order to compare the property difference of $Ni(OH)_2$ located on CNT and $Ni_3(HITP)_2$, as shown in Supplementary Scheme 1, we used two heterojunction models for DFT calculation. A vacuum region of 15 Å was added to avoid the interactions between adjacent images. As the radius of CNT in our work was larger than 10 nm, the curved surface of CNT was near to flat, meanwhile, in order to reduce the amount of calculation, we used graphene model to replace CNT. On the other hand, we built a cluster $Ni_{19}(OH)_{54}$ to represent $Ni(OH)_2$ grains in our work. Moreover, the Ni^{3+} in cluster was corresponding to the XPS results, and the diameter of the cluster was about 1.3 nm, which was close to the diameter of the confined $Ni(OH)_2$ observed under TEM.

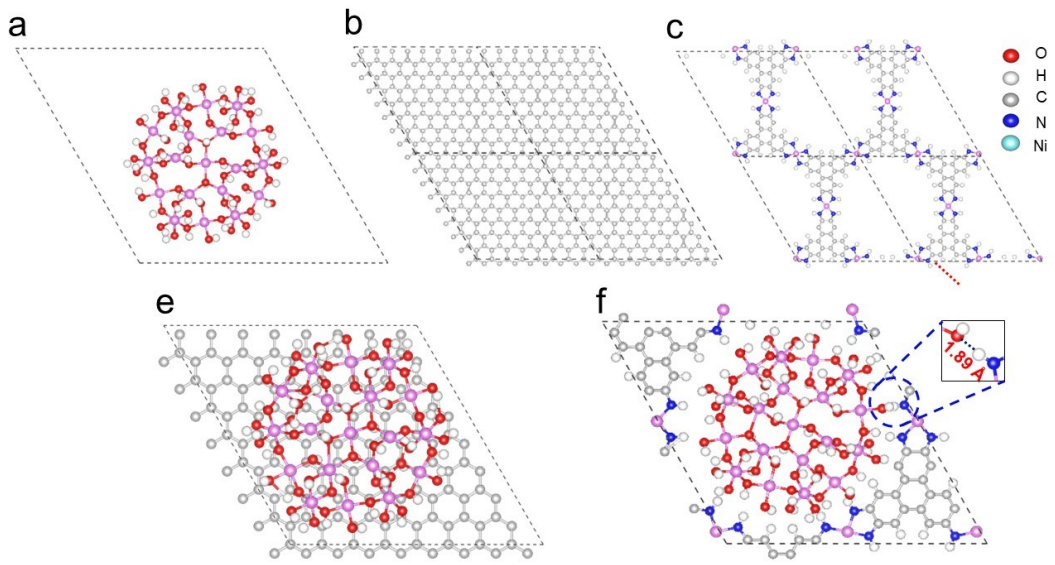

Supplementary Scheme 1 | The optimized geometric structure of (a) $Ni(OH)_2$, (b) graphene, (c) $Ni_3(HITP)_2$, (d) $Ni(OH)_2$@graphene and (e) $Ni(OH)_2$@$Ni_3(HITP)_2$.

Supplementary Note 4

Related Calculation Equations

The room temperature electrical conductivity (σ) of yarn was measured according to the four-wire method using a Keithley 2400.[7] Electrical conductivity was calculated using Equation 1:

$$\sigma = \frac{l}{RA} \quad (1)$$

where R (Ω) is the electrical resistance, A (cm^2) is the cross-sectional area, and l (cm) is the distance between the two inner electrodes.

The electrochemical properties of the YSCs were investigated by an electrochemical workstation (CHI 660E, CH Instruments Inc.), including cyclic voltammetry (CV), galvanostatic charge/discharge (GCD) and electrochemical impedance spectra (EIS) (from 0.01 Hz to 100 kHz) in two-electrode system. The cyclic performance was investigated with a CT 2001A battery program controlling test system (China-Land Co., Ltd). The specific capacitance, energy density and power density were calculated according to the reported equations.[8-9] The specific capacitance of a single yarn (C_s) was determined from CV test by Equation 2:

$$C_s = \frac{\int_{U_1}^{U_2} I\,dU + \int_{U_2}^{U_1} I\,dU}{S \times u \times (U_2 - U_1)} \quad (2)$$

where C_s (F/cm^2) is the specific areal capacitance of an individual electrode, S (cm^2) is the surface area of a single electrode, I (A) represents the instant current of CV curve, u (V/s) is scan rate, U_2 and U_1 (V) are high and low potential limit of CV test, respectively.

Galvanostatic charge/discharge (GCD) measurement at different current densities was performed to reveal information on capacitive performance of all prepared YSCs. The specific capacitance of a single yarn C_s (F/cm^2) was derived from Equation 3:

$$C_s = \frac{2 \times I \times t}{\Delta U \times S} \quad (3)$$

where I (A) is the discharge current, t (s) is the discharge time and ΔU (V) is potential window (U_2-U_1). The surface area of a single electrode S (cm^2) was expressed by Equation 4:

$$S = \pi DL \quad (4)$$

where D (cm) is the diameter of the yarn electrode measured from FESEM image and L (cm) is the length of two parallelly-laid yarns measured by a ruler. The energy density of a single yarn E_s (Wh/cm^2) was calculated from Equation 5:

$$E_s = \frac{C_s U^2}{2} \quad (5)$$

where C_s is obtained from Equation 3 and U (V) is the potential window. Value of the power density P_s (W/cm^2) of a single electrode was obtained from Equation 6:

$$P_s = \frac{E_s}{t} \quad (6)$$

where E_s (Wh/cm^2) was calculated by the Equation 5, t (s) is the discharge time from Equation 3. The specific energy density E_D (Wh/cm^2) and power density P_D (W/cm^2) of the whole device were obtained from Equation 5 and Equation 6:

$$E_D = \frac{E_s}{4} \quad (7)$$

$$P_D = \frac{P_s}{4} \quad (8)$$

Supplementary Figures

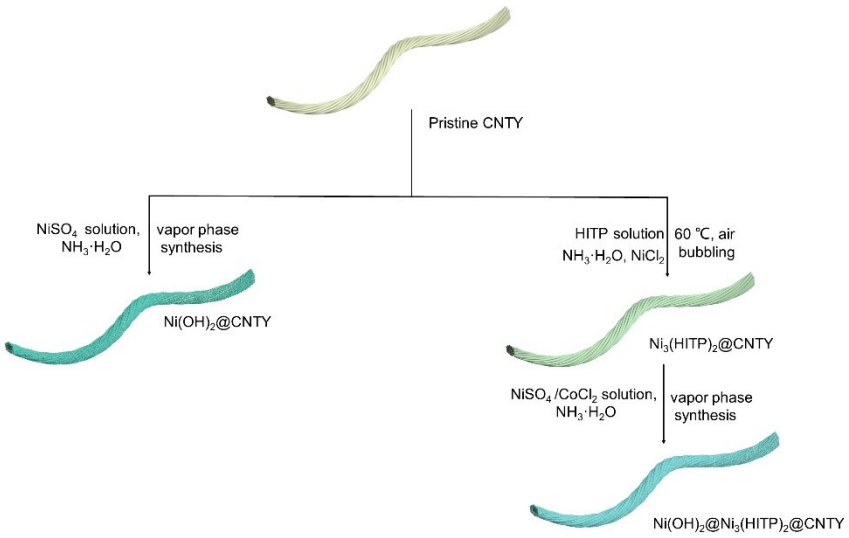

Supplementary Figure 1 | Schematic illustration for the preparation process of CNTY-based samples.

First, 2D-$Ni_3(HITP)_2$ nanolayer is *in-situ* grown onto CNT surface in CNTY. In this step, the pre-cleaned CNTY was immersed in HATP·6HCl ligand solution. Subsequently, ammonia ($NH_3·H_2O$) and nickel chloride ($NiCl_2$) were added into the mixed solution to construct coordinate bonds between ligands and nickel ions. Second, $Ni(OH)_2$ or $Co(OH)_2$ NPs were grown into the nanopores of $Ni_3(HITP)_2$ by vapor phase synthesis method. The prepared $Ni_3(HITP)_2$@CNTY was immersed in nickel sulfate ($NiSO_4$) solution to electrostatically attract Ni^{2+} or Co^{2+} precursors into 2D-$Ni_3(HITP)_2$ nanopores till $Ni(OH)_2$ or $Co(OH)_2$ NPs were confined in nanopores due to the geometrical constraint.[10] Then the prepared sample was thoroughly washed with DI water to remove residual superficial nickel ions.[11]

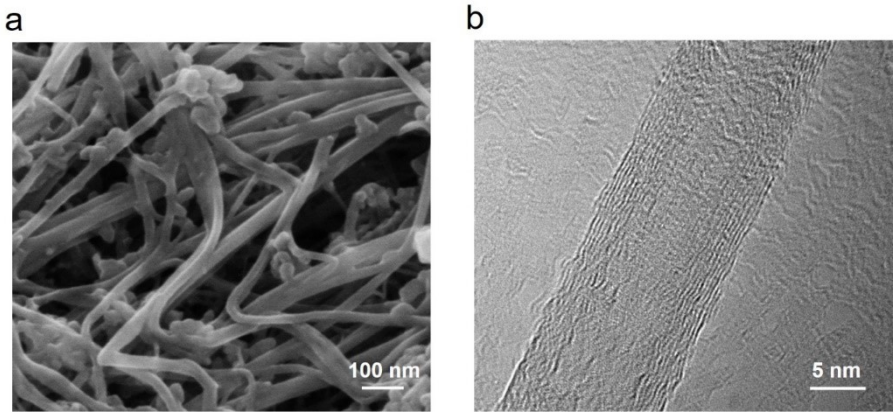

Supplementary Figure 2 | (a) FESEM image and (b) TEM image of pristine CNT.

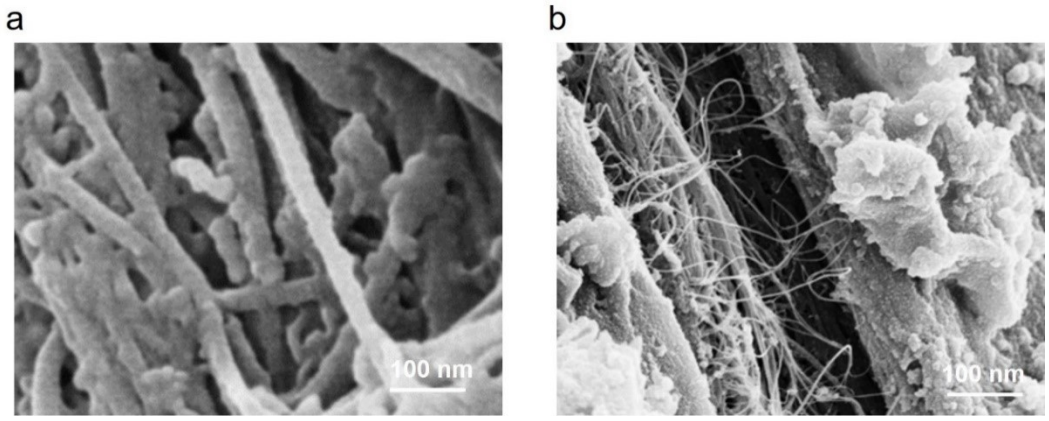

Supplementary Figure 3 | FESEM images of (**a**) $Ni_3(HITP)_2@CNT_{(2)}$ and (**b**) $Ni_3(HITP)_2@CNT_{(4)}$.

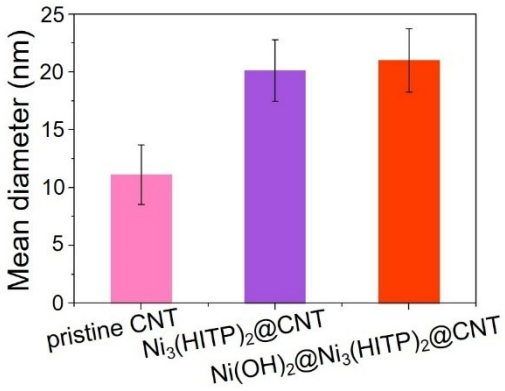

Supplementary Figure 4 | The mean diameter distribution of pristine CNT, $Ni_3(HITP)_2$@CNT and $Ni(OH)_2$@$Ni_3(HITP)_2$@CNT.

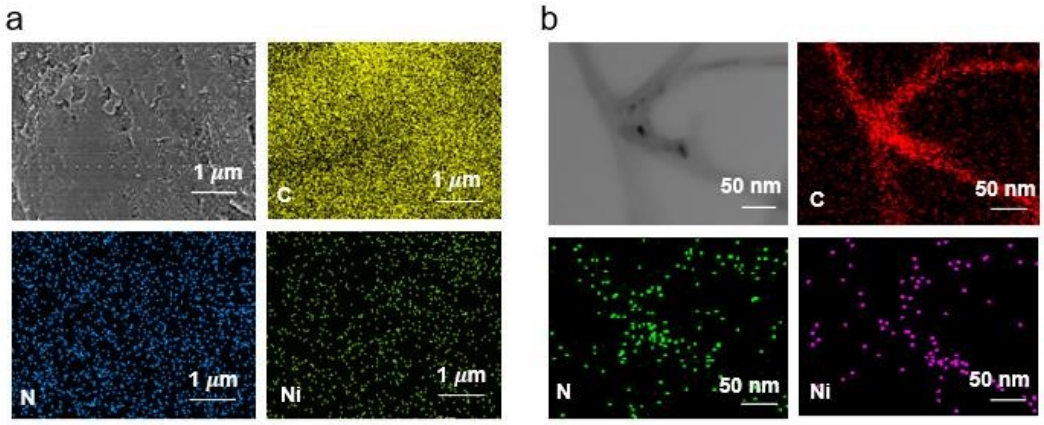

Supplementary Figure 5 | (**a**) FESEM-EDS and (**b**) TEM-EDS element mapping patterns of $Ni_3(HITP)_2$@CNT.

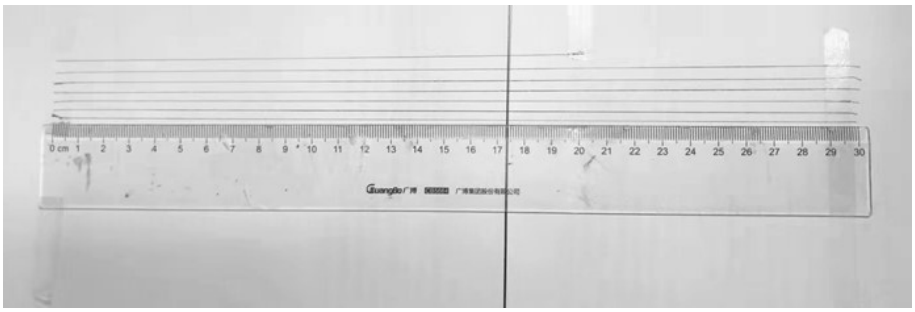

Supplementary Figure 6 | The photograph of a 200-cm long CNT-based yarn. The mass of 200-cm CNTY, $Ni_3(HITP)_2$@CNTY and $Ni(OH)_2$@$Ni_3(HITP)_2$@CNTY is 6.96 mg, 8.17 mg and 8.92 mg, respectively.

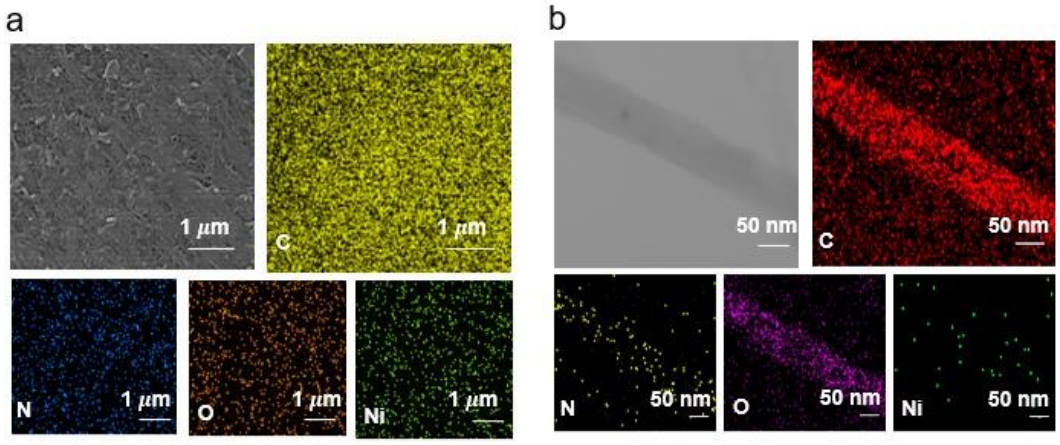

Supplementary Figure 7 | (**a**) FESEM-EDS and (**b**) TEM-EDS element mapping patterns of $Ni(OH)_2$@$Ni_3(HITP)_2$@CNT.

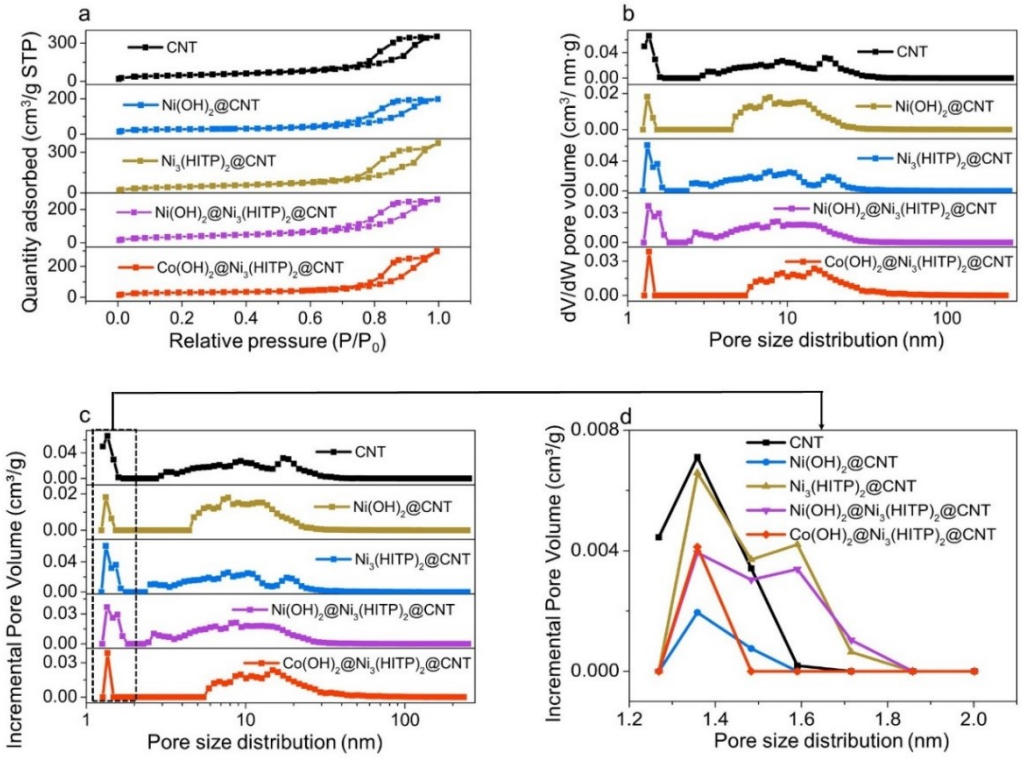

Supplementary Figure 8 | (**a**) N_2 adsorption/desorption isotherms and (**b-d**) the corresponding pore size distribution of CNT film-based samples.

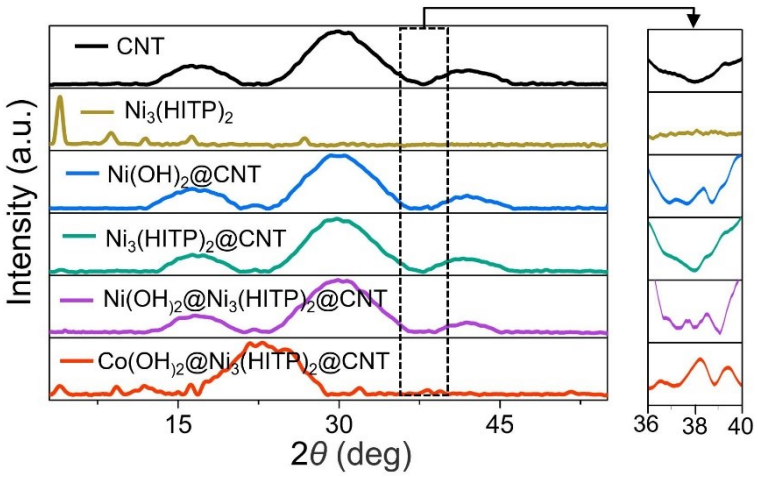

Supplementary Figure 9 | XRD patterns of CNT film-based samples from $2\theta = 36^{o}$ to $2\theta = 40^{o}$. Note: The CNT which forms CNTY and CNT film is not different.

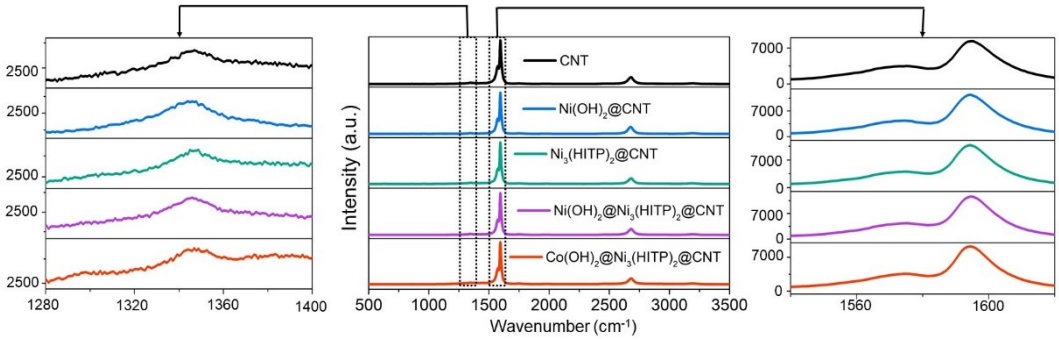

Supplementary Figure 10 | Raman spectra of all prepared CNT film-based samples. Note: (1) CNT films instead of CNTYs were used to synthesize five types of large samples for Raman spectra. (2) The left inset shows Raman spectra from 1280 cm^{-1} to 1400 cm^{-1}, the right inset shows Raman spectra from 1520 cm^{-1} to 1620 cm^{-1}.

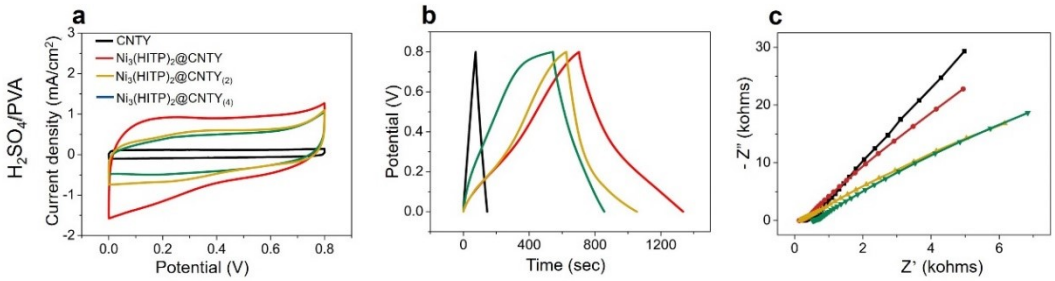

Supplementary Figure 11 | Electrochemical performance of CNTY based SCs in two-electrode system. (**a**) CV curves at 5 mV/s, (**b**) GCD curves at 0.1 mA/cm^2 and (**c**) EIS tests of CNTY-based SCs in 1 M H_2SO_4/PVA gel electrolyte.

For $Ni_3(HITP)_2$ modified CNTY electrodes, the CV measurements with EDLC behavior[12] reflect $Ni_3(HITP)_2$@CNTY SC has the biggest closed area in H_2SO_4/PVA electrolyte, leading to the highest areal specific capacitance (397.5 mF/cm^2) (Supplementary Figure 11a and Supplementary Figure 12a). According to GCD curves, $Ni_3(HITP)_2$@CNTY SC has the longest discharge time (1350.0 s) and a capacitance value of ~340.0 mF/cm^2 at 0.1 mA/cm^2 among all SCs (Supplementary Figure 11b and Supplementary Figure 12b). Furthermore, compared to the equivalent series resistance (ESR) of CNTY SC (271.9 Ω), $Ni_3(HITP)_2$@$CNTY_{(2)}$ SC (153.7 Ω) and $Ni_3(HITP)_2$@$CNTY_{(4)}$ SC (525.5 Ω), $Ni_3(HITP)_2$@CNTY SC shows the smallest ESR (132.3 Ω) (Supplementary Figure 11c) due to its high conductivity, expecting a fast charge transfer process. The C_A enhancement is attributed to the porous conducting $Ni_3(HITP)_2$ on CNT, which offers abundant ion-accessible active sites and facilitates charge transfer between electrode and electrolyte.[13] However, the excessive deposition of $Ni_3(HITP)_2$ on CNT is unfavorable for ion transport and storage due to the decreased ion-accessible surface area in denser structures (Supplementary Figure 3a-3b).[14-16]

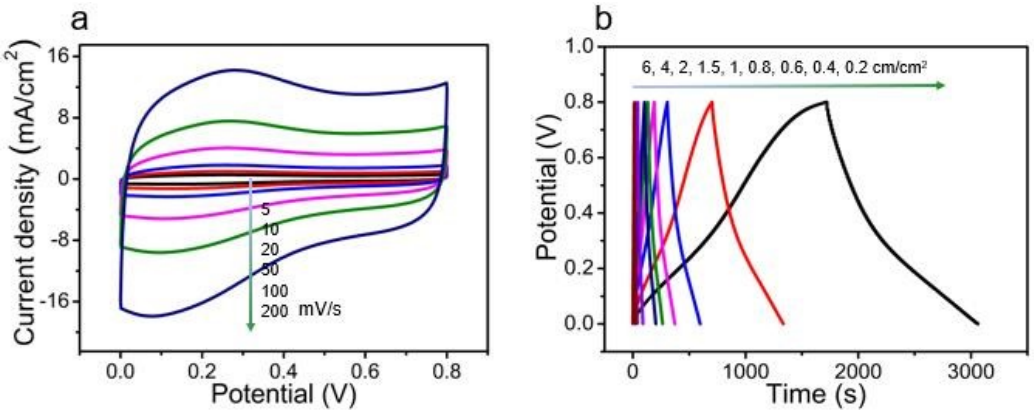

Supplementary Figure 12 | (**a**) CV and (**b**) GCD curves of $Ni_3(HITP)_2$@CNTY SC.

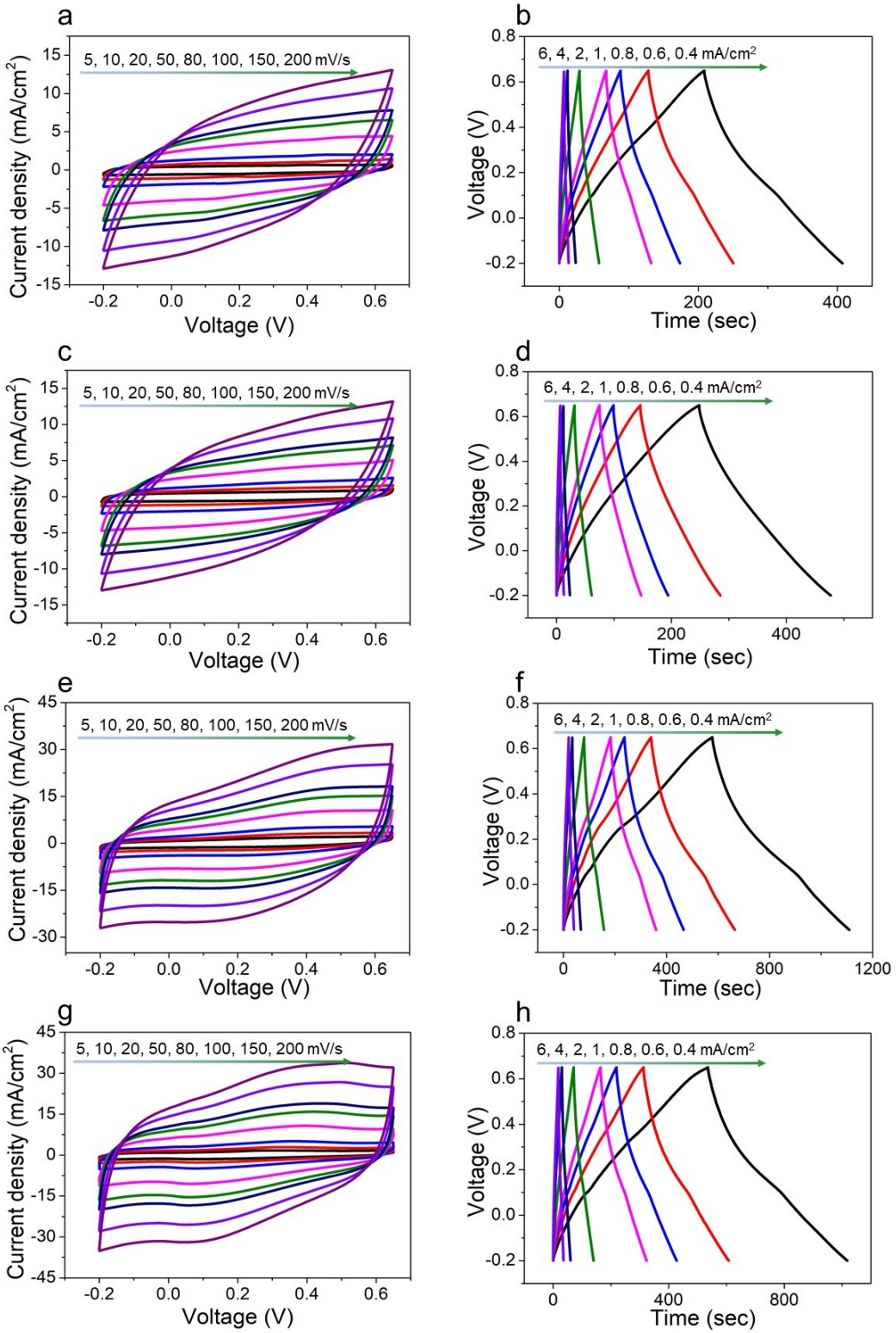

Supplementary Figure 13 | CV and GCD curves of (**a**, **b**) $Ni(OH)_2$@CNTY SC, (**c**, **d**) $Ni_3(HITP)_2$@CNTY SC, (**e**, **f**) $Ni(OH)_2$@$Ni_3(HITP)_2$@CNTY SC and (**g**, **h**) $Co(OH)_2$@$Ni_3(HITP)_2$@CNTY SC.

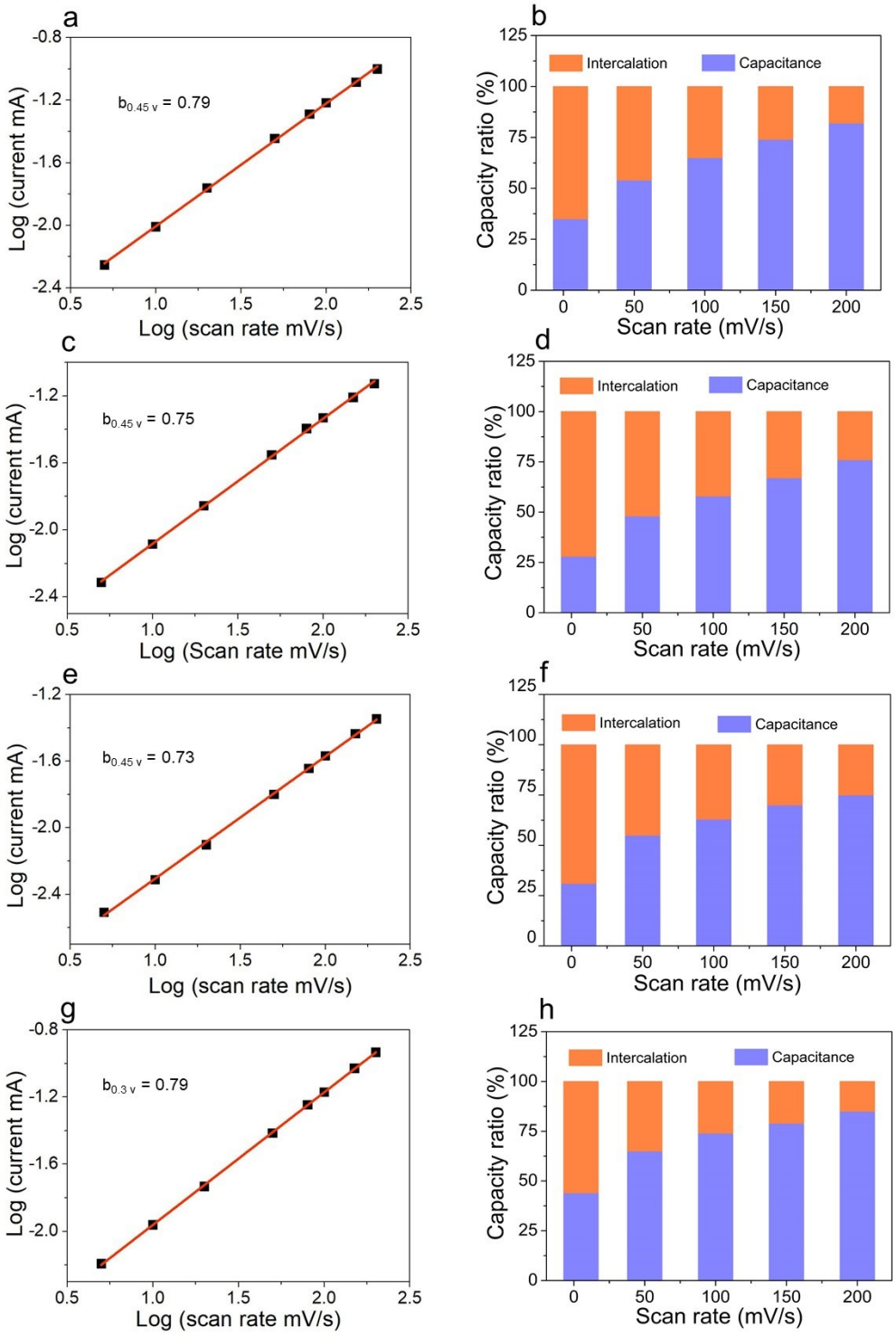

Supplementary Figure 14 | *b*-value and bar chart indicating the percentages of capacitive contribution of (**a**, **b**) $Ni(OH)_2$@CNTY SC, (**c**, **d**) $Ni_3(HITP)_2$@CNTY SC, (**e**, **f**) $Ni(OH)_2$@$Ni_3(HITP)_2$@CNTY SC and (**g**, **h**) $Co(OH)_2$@$Ni_3(HITP)_2$@CNTY SC from 5 to 200 mV/s.

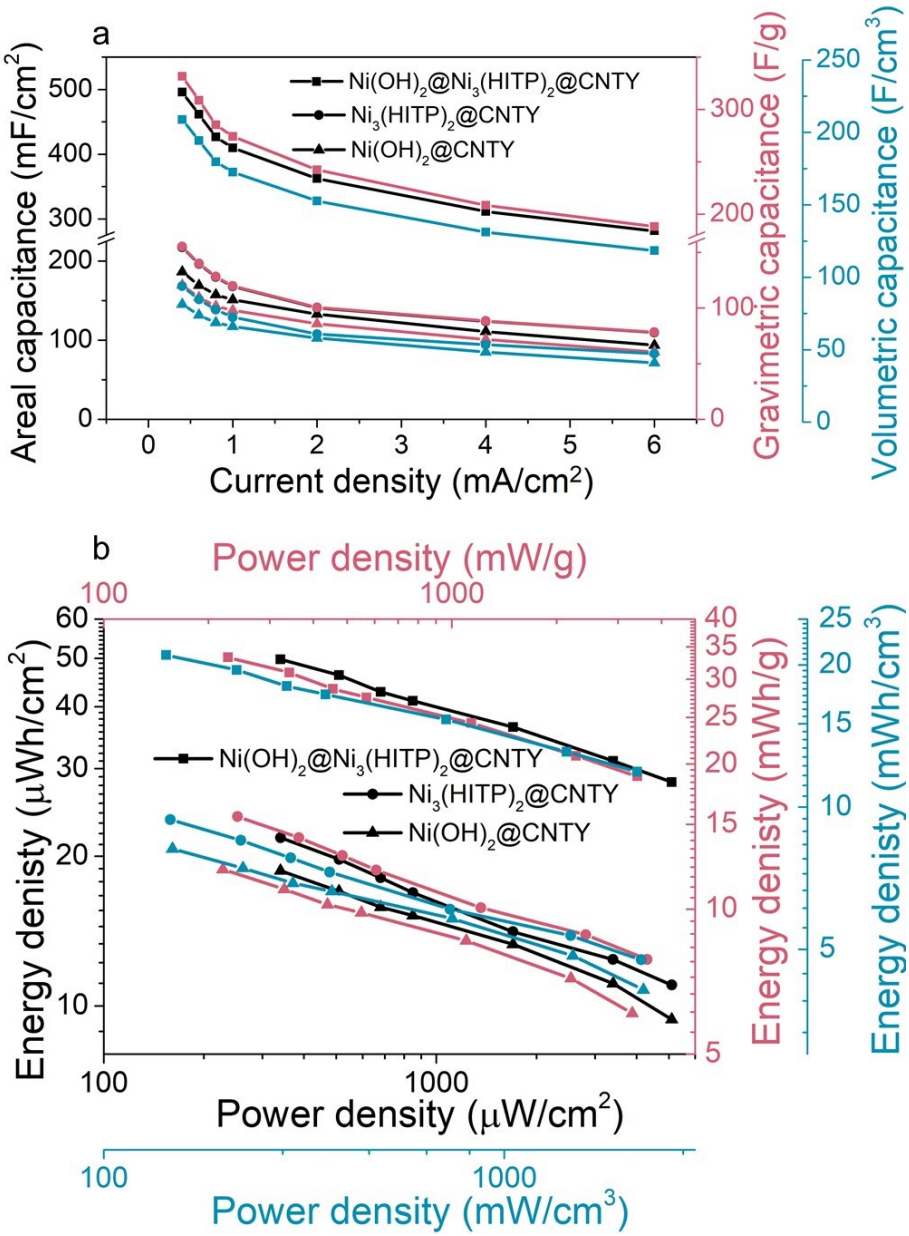

Supplementary Figure 15 | (**a**) The calculated capacitance of CNTY-based electrodes. (**b**) Energy density and power density of CNTY-based electrodes.

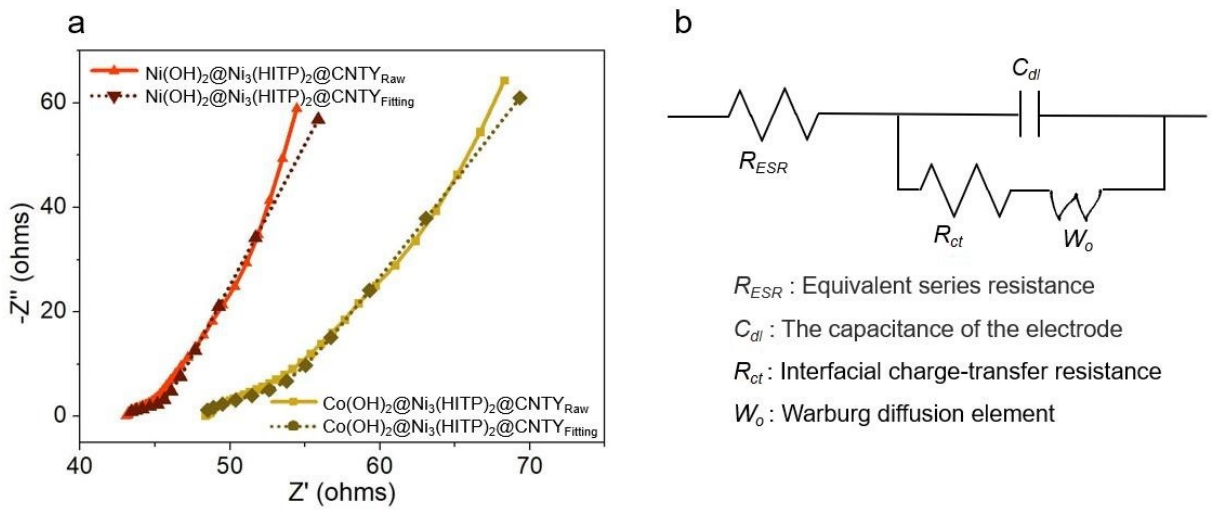

Supplementary Figure 16 | (**a**) Nyquist-plot of TMH NPs@$Ni_3(HITP)_2$@CNTY SCs with raw data as a solid line and fitting as short dot line. (b) Electrical equivalent circuit used for fitting the experimental EIS data. Note: The Warburg diffusion element W_o is a function of three parameters: *W-R*, the Warburg diffusion impedance; *W-T*, the diffusion time constant, and *W-P*, the phase factor ($0 < W\text{-}P < 1$).

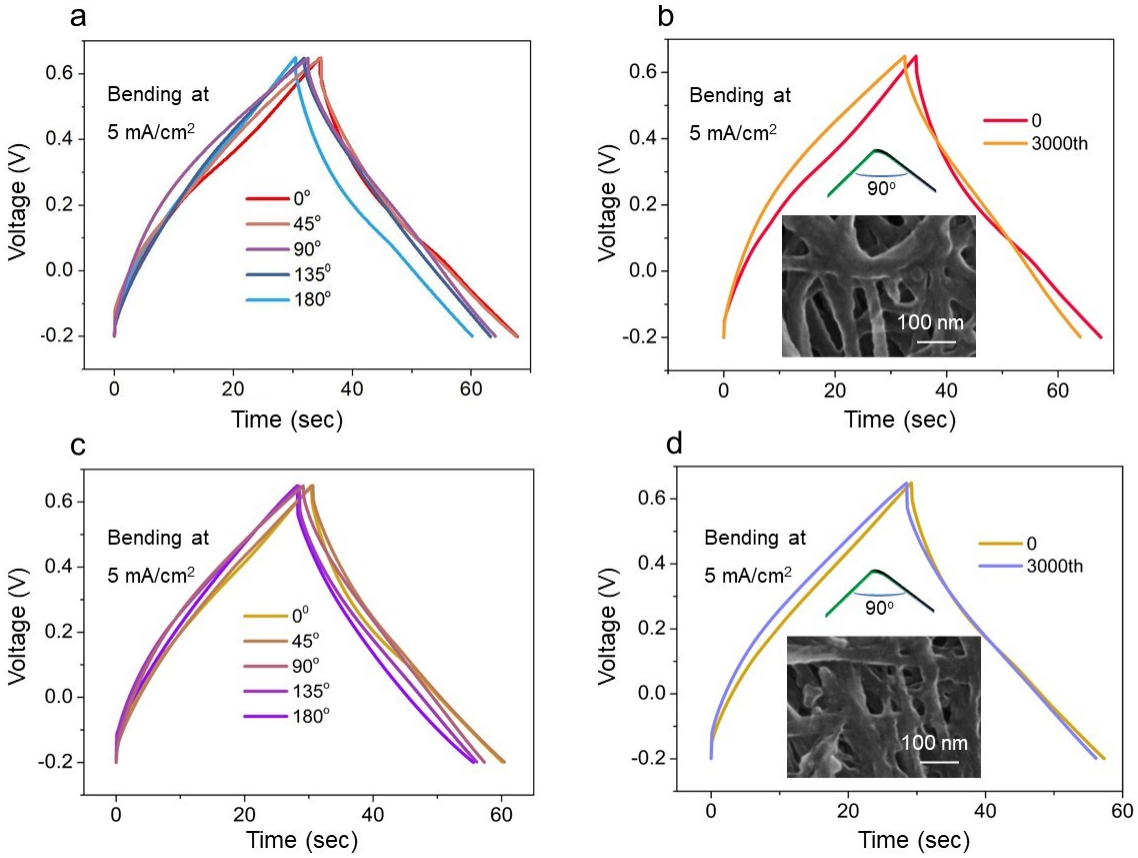

Supplementary Figure 17 | GCD curves of (**a**, **b**) $Ni(OH)_2@Ni_3(HITP)_2@CNTY$ SC and (**c**, **d**) $Co(OH)_2@Ni_3(HITP)_2@CNTY$ SC with different bending angles and after bending 3000 cycles at 90°. Notes: The insets of (b) and (d) are FESEM images of $Ni(OH)_2@Ni_3(HITP)_2@CNTY$ SC and $Co(OH)_2@Ni_3(HITP)_2@CNTY$ SC after bending 3000 cycles at 90°, respectively.

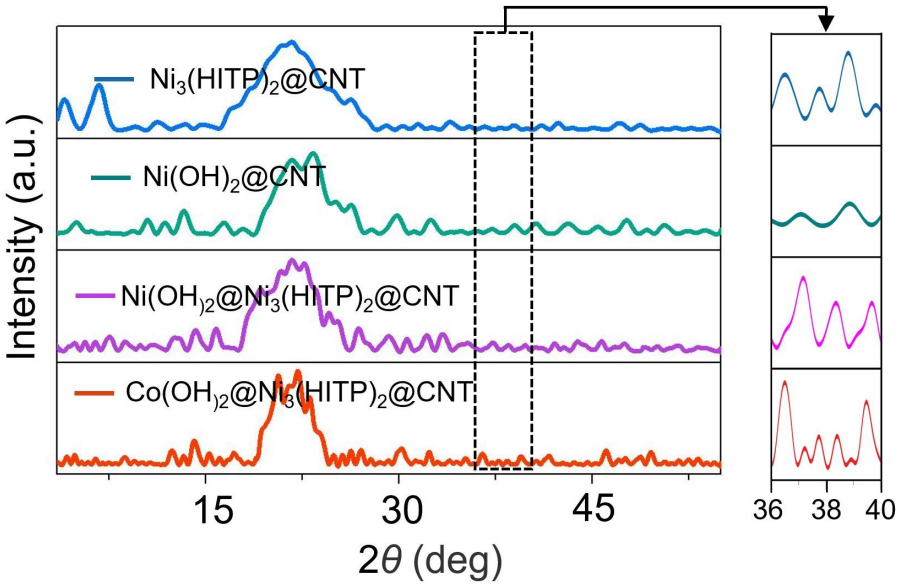

Supplementary Figure 18 | XRD patterns of CNT film-based samples after 10000 cycles in two-electrode system. Note: The CNT which forms CNTY and CNT film is not different.

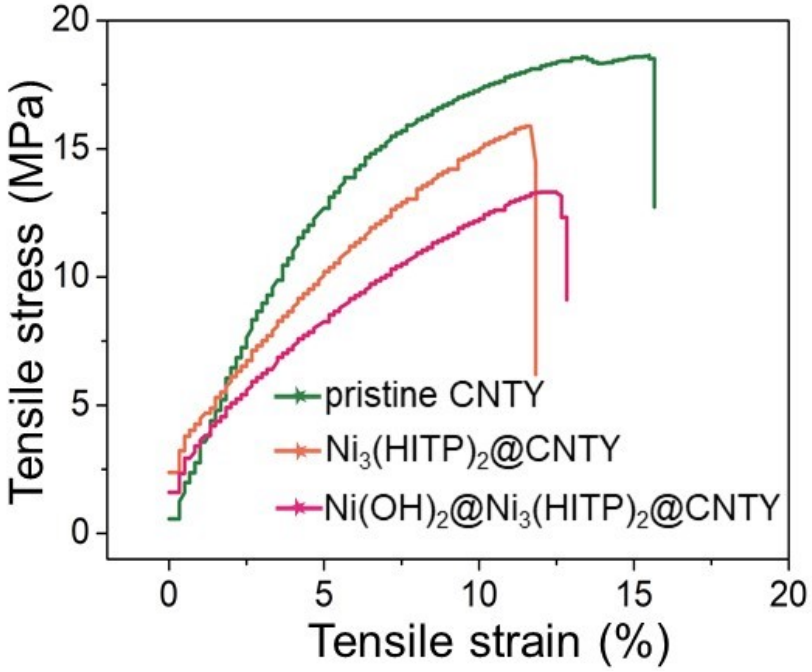

Supplementary Figure 19 | The mechanical property of CNTY-based samples.

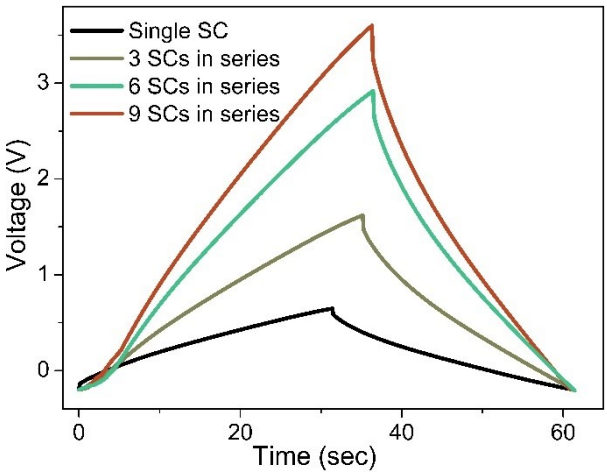

Supplementary Figure 20 | Galvanostatic charging/discharging curves of the assembled SCs connected in series.

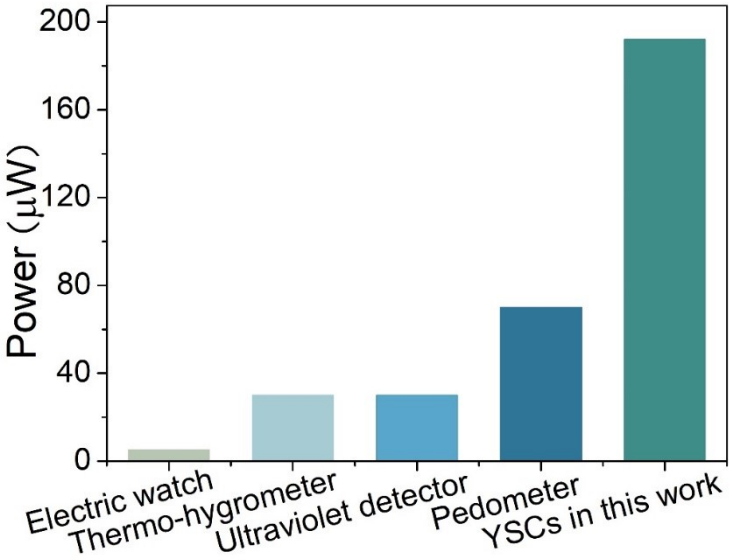

Supplementary Figure 21 | The power requirement of smart devices and the integrated YSC

Supplementary Table 1 | The conductivity of CNTY-based electrodes

Sample	pristine CNTY	$Ni_3(HITP)_2$ @CNTY	$Ni_3(HITP)_2$ @$CNTY_{(2)}$	$Ni_3(HITP)_2$ @$CNTY_{(4)}$	$Ni(OH)_2$ @CNTY	$Ni(OH)_2$@ $Ni_3(HITP)_2$ @CNTY
Conductivity (S/cm)	937.5	854.9	755.6	676.5	608.1	768.1

Supplementary Table 2 | Comparison of $Ni(OH)_2$-based symmetric supercapacitors

Electrode	Electrolyte	V	*i*	C	E	P	L	R
$Ni(OH)_2$@CCF-200[17]	KOH (aqueous)	1.40 V	0.25 A/g	131.43 F/g	35.78 mWh/g	350.00 mW/g	/	/
$Co(OH)_2$[18]	KOH (aqueous)	1.20 V	0.70 mA/cm^2 (0.1 A/g)	2.92 mF/cm^2	15.84 mWh/g	16800.00 mW/g	/	/
$Co(OH)_2$/graphene foam[19]	KOH (aqueous)	1.2 V	5.00 A/g	160.00 F/g	13.90 mWh/g	18000.00 mW/g	/	/
$Co(OH)_2$/stainless steel[19]				276.00 F/g	8.00 mWh/g	18000.00 mW/g	/	/
Zinc cobalt sulfide /$Ni(OH)_2$[20]	KOH/PVA (gel)	1.30 V	1.00 A/g	1276.00 F/g	74.93 mWh/g	650.00 mW/g	0.50mg/ cm^2	1300.00
graphene encapsulated $Ni(OH)_2$ nanosheet transparent film[21]	KOH/PVA (gel)	1.00 V	0.10 mA/cm^2	18.90 mF/cm^2	2.43 mWh/cm^3	196.00 mW/cm^3	0.0315 mg/cm^2	6222.22
Ag nanowire/ $Ni(OH)_2$ nanosheet[22]	KOH/PVA (gel)	0.50 V	0.50 A/g	78.00 F/g	2.71 mWh/g	143.47 mW/g	0.80 mg/cm^2	179.63
$K_2Ti_4O_9$@$Ni(OH)_2$/Ti[23]	KOH/PVA (gel)	0.80 V	0.40 mA/cm^2	2.25 mF/cm^2	0.72 mWh/cm^2	0.16 mW/cm^2	/	/
$Ni(OH)_2$/$NiMoO_4$[24]	tetraethylam -monium hydroxide/ PVA (gel)	0.50 V	0.20 mA/cm^2	2.60 mF/cm^2	0.12 μWh/cm^2	100.00 μW/cm^2	/	/
β-$Ni(OH)_2$/graphene[25]	KOH/PVA (gel)	0.6 V	0.10 mA/cm^2	2.12 mF/cm^2	/	/	/	/
$Ni(OH)_2$@Ni_3(HITP)$_2$@CNTY	**KOH/PVA (gel)**	**0.85 V**	**0.40 mA/cm^2**	**496.00 mF/cm^2**	**49.80 μWh/cm^2**	**340.00 μW/cm^2**	**0.10 mg/cm^2 (3.75 μg/cm)**	**3400.00**
				331.80 F/g	**33.31 mWh/g**	**227.45 mW/g**		**2274.50**
				208.91 F/cm^3	**20.98 mWh/cm^3**	**143.20 mW/cm^3**		**1432.0**

Note: The details of the table are as following:

(1) V represents potential window, *i* represents current density, C represents specific capacitance, E represents energy density, P represents power density, L represents mass loading of $Ni(OH)_2$, R represents power density /mass loading of $Ni(OH)_2$.

(2) The potential window of the electrode is the voltage of GCD test, the energy density and power density are calculated from the specific capacitance of single electrode.

(3) The mass loading is only calculated from the mass of $Ni(OH)_2$.
(4) The definition of Power density/Mass loading of $Ni(OH)_2$ is that the amount of change in power density per unit mass loading. Hypothesis that the higher the mass loading of $Ni(OH)_2$, the higher the experimental power density. Then the conclusion can be found that the higher the value of the ratio, the higher the experimental contribution rate of $Ni(OH)_2$ for power density.
(5) The mass loading of $Ni(OH)_2$ in our work: The mass of 200-cm long $Ni(OH)_2$@$Ni_3(HITP)_2$@CNTY and $Ni_3(HITP)_2$@CNTY is 8.92 mg and 8.17 mg, respectively. The mean diameter of $Ni(OH)_2$@$Ni_3(HITP)_2$@CNTY is 120 μm. So, the mass of $Ni(OH)_2$ is equal to 8.92 mg - 8.17 mg = 0.75 mg, the area of the $Ni(OH)_2$@$Ni_3(HITP)_2$@CNTY is equal to 200 cm x 120 μm x π = 7.54 cm^2. Thus the mass loading of $Ni(OH)_2$ in our work is 0.75 mg/7.54 cm^2 = 0.10 mg/cm^2.

Supplementary Table 3 | Resistance values obtained by fitting the equivalent circuit to the EIS plots for TMH NPs@$Ni_3(HITP)_2$@CNTY SCs

Sample	$Ni(OH)_2$@$Ni_3(HITP)_2$@CNTY	$Co(OH)_2$@$Ni_3(HITP)_2$@CNTY
R_{ESR} (Ω)	42.9	48.3
R_{ct} (Ω)	1E-3	1E-3
W-R (Ω)	8.4	18.0
W-T (Ω)	5E-4	1E-3
W-P (Ω)	0.4	0.4

Supplementary References:

1. Chen, L.; Kim, J.; Ishizuka, T.; Honsho, Y.; Saeki, A.; Seki, S.; Ihee, H.; Jiang, D. L., Noncovalently Netted, Photoconductive Sheets with Extremely High Carrier Mobility and Conduction Anisotropy from Triphenylene-Fused Metal Trigon Conjugates. *J. Am. Chem. Soc.* **2009,** *131* (21), 7287-7292.
2. Kresse, G.; Hafner, J., Ab initio molecular dynamics for open-shell transition metals. *Phys. Rev., B Condens.* **1993,** *48* (17), 13115-13118.
3. Kresse, G.; Furthmuller, J., Efficiency of ab-initio total energy calculations for metals and semiconductors using a plane-wave basis set. *Comput. Mater. Sci.* **1996,** *6* (1), 15-50.
4. Perdew, J. P.; Burke, K.; Ernzerhof, M., Generalized gradient approximation made simple. *Phys. Rev. Lett.* **1996,** *77* (18), 3865-3868.
5. Kresse, G.; Joubert, D., From ultrasoft pseudopotentials to the projector augmented-wave method. *Phys. Rev. B* **1999,** *59* (3), 1758-1775.
6. Heyd, J.; Scuseria, G. E.; Ernzerhof, M., Hybrid functionals based on a screened Coulomb potential. *J. Chem. Phys.* **2003,** *118* (18), 8207-8215.
7. Kim, B.-H.; Yang, K. S.; Kim, Y. A.; Kim, Y. J.; An, B.; Oshida, K., Solvent-induced porosity control of carbon nanofiber webs for supercapacitor. *J. Power Sources* **2011,** *196* (23), 10496-10501.
8. Zheng, B.; Huang, T.; Kou, L.; Zhao, X.; Gopalsamy, K.; Gao, C., Graphene fiber-based asymmetric micro-supercapacitors. *J. Mater. Chem. A* **2014,** *2* (25), 9736-9743.
9. Yu, D.; Goh, K.; Wang, H.; Wei, L.; Jiang, W.; Zhang, Q.; Dai, L.; Chen, Y., Scalable synthesis of hierarchically structured carbon nanotube-graphene fibres for capacitive energy storage. *Nat. Nanotechnol.* **2014,** *9* (7), 555-562.
10. Juan-Alcañiz, J.; Gascon, J.; Kapteijn, F., Metal–organic frameworks as scaffolds for the encapsulation of active species: state of the art and future perspectives. *J. Mater. Chem. A* **2012,** *22* (20), 10102-10118.
11. Wang, T.; Farajollahi, M.; Henke, S.; Zhu, T.; Bajpe, S. R.; Sun, S.; Barnard, J. S.; Lee, J. S.; Madden, J. D. W.; Cheetham, A. K.; Smoukov, S. K., Functional conductive nanomaterials via polymerisation in nano-channels: PEDOT in a MOF. *Mater. Horizons* **2017,** *4* (1), 64-71.
12. Perera, S. D.; Patel, B.; Nijem, N.; Roodenko, K.; Seitz, O.; Ferraris, J. P.; Chabal, Y. J.; Balkus, K. J., Vanadium Oxide Nanowire-Carbon Nanotube Binder-Free Flexible Electrodes for Supercapacitors. *Adv. Energy Mater.* **2011,** *1* (5), 936-945.
13. Zhang, L.; Chen, H.; Bai, X.; Wang, S.; Li, L.; Shao, L.; He, W.; Li, Y.; Wang, T.; Zhang, X.; Chen, J.; Fu, Y., Fabrication of 2D metal-organic framework nanosheet@fiber composites by spray technique. *Chem. Commun.* **2019,** *55* (57), 8293-8296.
14. Ma, J.; Li, J.; Guo, R.; Xu, H.; Shi, F.; Dang, L.; Liu, Z.; Sun, J.; Lei, Z., Direct growth of flake-like metal-organic framework on textile carbon cloth as high-performance supercapacitor electrode. *J. Power Sources* **2019,** *428*, 124-130.
15. Qi, K.; Hou, R.; Zaman, S.; Qiu, Y.; Xia, B. Y.; Duan, H., Construction of Metal-Organic Framework/Conductive Polymer Hybrid for All-Solid-State Fabric Supercapacitor. *ACS Appl. Mater. Interfaces* **2018,** *10* (21), 18021-18028.
16. Liu, C.; Yu, Z.; Neff, D.; Zhamu, A.; Jang, B. Z., Graphene-Based Supercapacitor with an Ultrahigh Energy Density. *Nano Lett.* **2010,** *10* (12), 4863-4868.
17. Xia, T.; Zhang, X.; Zhao, J.; Li, Q.; Ao, C.; Hu, R.; Zheng, Z.; Zhang, W.; Lu, C.; Deng, Y., Flexible and Conductive Carbonized Cotton Fabrics Coupled with a Nanostructured Ni(OH)2 Coating for High Performance Aqueous Symmetric Supercapacitors. *ACS Sustain. Chem. Eng.* **2019,** *7* (5), 5231-5239.

18. Jagadale, A. D.; Kumbhar, V. S.; Dhawale, D. S.; Lokhande, C. D., Performance evaluation of symmetric supercapacitor based on cobalt hydroxide [Co(OH)2] thin film electrodes. *Electrochim. Acta* **2013,** *98*, 32-38.

19. Patil, U. M.; Lee, S. C.; Sohn, J. S.; Kulkarni, S. B.; Gurav, K. V.; Kim, J. H.; Kim, J. H.; Lee, S.; Jun, S. C., Enhanced Symmetric Supercapacitive Performance of Co(OH)2 Nanorods Decorated Conducting Porous Graphene Foam Electrodes. *Electrochim. Acta* **2014,** *129*, 334-342.

20. Syed, J. A.; Ma, J.; Zhu, B.; Tang, S.; Meng, X., Hierarchical Multicomponent Electrode with Interlaced Ni(OH)2

Nanoflakes Wrapped Zinc Cobalt Sulfide Nanotube Arrays for Sustainable High-Performance Supercapacitors. *Adv. Energy Mater.* **2017,** *7* (22), 1701228-1701240.

21. Li, N.; Huang, X.; Li, R.; Chen, Y.; Li, Y.; Shi, Z.; Zhang, H., Pseudocapacitive Transparent/Flexible Supercapacitor based on Graphene wrapped Ni(OH) 2 Nanosheet Transparent Film Produced using Scalable Bio-inspired Methods. *Electrochim. Acta* **2016,** *219*, 61-69.

22. Du, H.; Pan, Y.; Zhang, X.; Cao, F.; Wan, T.; Du, H.; Joshi, R.; Chu, D., Silver nanowire/nickel hydroxide nanosheet composite for a transparent electrode and all-solid-state supercapacitor. *Nanoscale Adv.* **2019,** *1* (1), 140-146.

23. Zhou, W.; Liu, X.; Sang, Y.; Zhao, Z.; Zhou, K.; Liu, H.; Chen, S., Enhanced performance of layered titanate nanowire-based supercapacitor electrodes by nickel ion exchange. *ACS Appl. Mater. Interfaces* **2014,** *6* (6), 4578-4586.

24. Feng, Y.; Liu, L.; Liang, J.; Yao, W.; Tian, B.; Jiang, C.; Wu, W., Ni(OH)2/NiMoO4 nanoplates for large-scale fully-printed flexible solid-state supercapacitors. *J. Power Sources* **2019,** *433*, 126676-126684.

25. Xie, J.; Sun, X.; Zhang, N.; Xu, K.; Zhou, M.; Xie, Y., Layer-by-layer β-Ni(OH)2/graphene nanohybrids for ultraflexible all-solid-state thin-film supercapacitors with high electrochemical performance. *Nano Energy* **2013,** *2* (1), 65-74.